ENGINEERING Information Technology & Electronic Engineering
https://www.academax.com/EITEE; https://www.engineering.org.cn
https://ieeexplore.ieee.org/xpl/RecentIssue.jsp?punumber=11344065
E-mail: eng.itee@zju.edu.cn

Engineering Journals
Available on IEEE Xplore®

Research Article

https://doi.org/10.1631/ENG.ITEE.2025.0024

Energy dynamics and circuit implementation for a neuron with a memcapacitive membrane

Binchi WANG[1,2], Yitong GUO[3], Guodong REN[1,2], Jun MA[2]✉

[1]*School of Microelectronics Industry-Education Integration, Lanzhou University of Technology, Lanzhou 730050, China*
[2]*Department of Physics, Lanzhou University of Technology, Lanzhou 730050, China*
[3]*School of Mathematics, North University of China, Taiyuan 030051, China*

Abstract: The output voltages for the capacitive elements of a neural circuit model can be mapped into dimensionless capacitive variables, which present firing patterns similar to the membrane potentials detected in biological neurons. The inclusion of a memcapacitor also enables consideration of membrane deformation effects, enhancing the model's capacity to simulate neuronal behavior across varying physiological and environmental conditions. In this study, a capacitor and a memcapacitor are connected through a linear resistor in parallel with other electric components in different branch circuits composed of an inductor and a nonlinear resistor. The electrical activities in a neuron with a double-layer membrane and two capacitive variables are discussed in detail after converting the nonlinear equations for the neural circuit into a theoretical neuron model. A dimensionless neuron model and its corresponding energy function are derived. The field energy function for the neural circuit is converted into an equivalent Hamilton energy function and further validated via the Helmholtz theorem. Furthermore, the average value of energy serves as an indicator for predicting stochastic resonance, as supported by analyzing the distribution of the coefficient of variation. The neuronal firing patterns are shown to be energy-dependent. An adaptive control strategy is proposed to regulate mode transitions in electrical activities of the neuron. An analog equivalent circuit is constructed to experimentally verify the numerical results, thereby supporting the reliability of the proposed neuron model.

Key words: Neural circuit; Neuron model; Hamilton energy; Memcapacitor; Coherence resonance

1 Introduction

The human brain comprises approximately 10^{11} neurons interconnected by roughly 10^{14} synapses (Herculano-Houzel, 2009). Complex network studies show that these networks exhibit small-world and modular structures with highly connected hub regions, which support efficient information processing and robust dynamics (Bullmore and Sporns, 2009). Inspired by these architectures, neuromorphic computing has become a challenge that aims to emulate the brain's massively parallel, low-power, and fault-tolerant operation (Indiveri et al., 2013; Beilliard and Alibart, 2021; Huang et al., 2021). Fast and effective signal processing in artificial neural networks is worthy of investigation in terms of model approach and algorithm reliability. In contrast, conventional von Neumann architectures, with strictly separated memory and processing units, incur a severe data "traffic jam" (memory bottleneck) and high energy cost when scaled to brain-like tasks. To overcome this, neuromorphic systems collocate memory and computation (for example, via memristive synapses) so that the weights and processing occur in place (Dong et al., 2021; Li Y and Shen, 2022; Li JY et al., 2023).

From a physical perspective, the membrane potentials of neurons can be effectively modeled by using capacitive components such as traditional capacitors and memcapacitors, whose main characteristics are electric field and charge levels associated with field energy. Modeling the electrical behavior of neurons has a long history, with simplified theoretical models capturing key neuronal features such as spiking, excitability, and bistability, while remaining analytically tractable (Cebrián-Lacasa et al., 2024). In particular, the FitzHugh–Nagumo (FHN) model, introduced in the early 1960s, is a canonical two-variable excitable cell model that reproduces relaxation oscillations, bistability, and excitability to external stimuli (FitzHugh, 1961). As one of the foundational reduced models, FHN condenses the complex Hodgkin–Huxley system into a tractable form amenable to analysis and experimental interpretation. In recent

✉ Jun MA, hyperchaos@163.com
Binchi WANG, https://orcid.org/0009-0004-6919-2503
Yitong GUO, https://orcid.org/0000-0001-7509-3174
Jun MA, https://orcid.org/0000-0002-6127-000X
CLC number: TN710; O59

Received: Sept. 8, 2025; Revision accepted: Oct. 23, 2025;
Crosschecked: Jan. 5, 2026; Published online: Jan. 26, 2026

decades, the FHN model and its improved versions have served as a theoretical and experimental approach tested for understanding excitable media and neuronal synchronization, including studies on coupled pairs and pattern formation (Yanagita et al., 2005; Plotnikov and Fradkov, 2019; Scialla et al., 2021). Coupled FHN neurons have been extensively analyzed for their synchronization behavior, revealing multi-stability, phase-repulsive and phase-attractive regimes, and the onset of complex firing patterns, including cyclic and chaotic dynamics. Extensions to diffusive and boundary-coupled networks uncovered rich spatiotemporal structures, such as Turing instabilities, spiral waves, and chimera states, driven by diffusion, time delays, and network topology (Quininao and Touboul, 2020; Tah et al., 2021; Ji and Mao, 2024; Wang HL et al., 2025). Recent work has even demonstrated synchronization mode transitions, chimera-like dynamics, and bifurcation delays in spatially extended FHN networks, highlighting their continued relevance in modern nonlinear neural modeling (Plotnikov and Fradkov, 2016; Gerster et al., 2020).

Concurrently, novel electronic devices have been incorporated into neuromorphic circuits to better mimic neural function. In particular, metal-oxide memristors (resistive memory devices) can emulate synaptic plasticity and neuronal firing behaviors (Prezioso et al., 2015; Zidan et al., 2018; Deswal et al., 2019; Tian et al., 2025). They have been used to implement integrate-and-fire spiking dynamics and spike-timing-dependent plasticity (STDP) in hardware arrays (Di Ventra et al., 2009; Khacef et al., 2023; Tomassoli et al., 2024) and show important application in building dense crossbar neural networks (Prezioso et al., 2016; Busygin et al., 2025). More recently, "memelements" beyond memristors, notably memcapacitors (capacitors with memory), have attracted interest because they can both store energy and exhibit history dependence (Romero et al., 2021; Ge et al., 2025a). These two kinds of memristors are considered higher-order nonlinear resistors with charge-dependent or magnetic flux-dependent resistance or memductance. The linear part consumes Joule heat, while the remaining higher-order term in the memristive function describes the field effect of the memristor. In the general approach of memristor-coupled nonlinear circuits, additive branch circuits incorporated with memristive elements are connected in parallel to the capacitive and inductive elements in other branch circuits, and the dynamics of developed memristive models show dependence on the initials and multi-stability (Budhathoki et al., 2013; Minati et al., 2020; Isah and Bilbault, 2022; Shao et al., 2024, 2025). Memristors can connect a voltage source for generating electric stimuli within a specific frequency band (Xie et al., 2024), and the filtered signals are very similar to realistic signals imposed on the nervous system. A hybrid ion channel (Yu et al., 2025) can be designed by connecting a memristor to an inductor in series, and continuous energy exchange is helpful in triggering stable firing activities in the neural circuit. Most importantly, a memristor can replace the capacitor, inductor, and even nonlinear resistor in the neural circuit. For example, a breakdown in the capacitor or inductor, or non-availability of some electric components, including capacitors or induction coils in the neural circuits, will terminate the signal processing and energy exchange, but some recent studies have confirmed that incorporation of a memristor can enhance energy exchange, enabling the neural circuit to present similar firing patterns without using any capacitors or inductors (Guo et al., 2024; Yang et al., 2024d; Lei et al., 2025).

Memcapacitors add the ability to recover and modulate energy flows in a circuit, potentially yielding more bio-plausible neuron models (Zheng et al., 2022). For example, Li PY and Li (2025) replaced the FHN circuit's ordinary capacitor with a charge-controlled memcapacitor and found that the resulting neuron exhibits a rich repertoire of dynamical regimes, including tonic spiking, subthreshold oscillations, bursting and bi-stability, and transitions among periodic, multi-periodic, and chaotic firing, depending on the stimuli and initial conditions. Ge et al. (2025b) similarly modeled an FHN neuron with a Miller-effect memcapacitor, derived an equivalent Hamilton, and showed that the system's impedance and firing behavior depend on the flux history. They observed memory-dependent impedance, state-dependent energy firing, and even noise-induced resonance peaks in the energy dynamics. Shi et al. (2024) introduced a memristor-coupled memcapacitor synapse in a Hopfield neural network, where the novel memcapacitor-synapse element exhibited complex plastic dynamics and extreme multistability, demonstrating brain-like "bionic" memory behavior of the combined memristor–memcapacitor structure. Studies on chaotic circuits combining memristor and memcapacitor elements have reported extreme multistability and complex phase dynamics suitable for neuromorphic tasks (Chen et al., 2023; Han et al., 2024). Cellular neural networks leveraging memcapacitor elements suggest promising applications in associative memory and cryptography (Wang X et al., 2025).

Beyond single-membrane configurations in which the neuron model has one capacitive variable for the membrane potential, the concept of neuron models containing a double-layer membrane has been explored to mirror the biophysical complexity of lipid bilayers and extracellular field interactions. These neuron models have two capacitive variables (Li YN et al., 2024a; Wang BC et al., 2024, 2025; Wang HL et al., 2025), which measure the energy characteristic and potential diversity for the inner and outer cell membrane, and two capacitors are coupled in parallel with other branch circuits in the neural circuits. Guo et al. (2023) suggested a neuron model containing a memristive membrane and its circuit implementation of two capacitive variables expressed by coupling two capacitors via a memristor. Yang et al. (2024c) simulated dynamics in a memristor-mediated double-membrane neuron, highlighting the role of inter-membrane energy gradients in coherence resonance and adaptive firing. Song et al. (2025) discussed the energy dynamics and resonance in a neuron holding with a memristive channel and membranes. These double-membrane models reveal how inter-membrane coupling and energy gradients can regulate excitability and synchronous firing in networks. Unlike previous double-membrane models, where both layers were represented by conventional capacitors, our study introduces a memcapacitor as the outer membrane. Compared with existing memristive FHN models that adjust firing mainly through resistive memory effects, the memcapacitor provides a charge- and energy-dependent mechanism, allowing the outer membrane to exhibit memory-dependent capacitance and deformation under external stimuli. As a result, it becomes the key factor in energy regulation and stochastic resonance, thereby highlighting the novelty of our approach. Recent achievements have introduced discrete memristive neuron models that incorporate magnetic induction and electromagnetic effects, exhibiting rich dynamical behaviors such as multi-stability, chaotic bursting, and bifurcation transitions consistent with FHN mechanisms

(Li YN et al., 2024b; Yang et al., 2024a; Song and Yang, 2025). Comprehensive discussions of neural circuit dynamics from a physical perspective are available in recent reviews (Ma, 2023; Panda et al., 2024; Yang et al., 2024b).

In the present study, we continue this trajectory by constructing a double-membrane FHN-type neuron in which one membrane is represented by a conventional linear capacitor and the other by a memcapacitor, with a resistor between them (modeling the intramembrane dielectric). By incorporating a memcapacitor into the model, we simulate a deformable membrane structure that dynamically adjusts its capacitive state in response to electrical and energetic fluctuations. This not only enhances the biophysical plausibility of the model, but also allows for dynamic adaptation akin to real cellular membranes responding to external stimuli. To assess the influence of uncertainty and an external electromagnetic field on neuronal activities, a noisy disturbance is introduced, revealing the presence of stochastic resonance. In addition, we propose a self-adaptive parameter evolution law to investigate regulatory behavior in the memcapacitive neuron model. The resulting dynamical features and associated energy profiles are systematically analyzed.

2 Neural circuit and model description

In this model, the architecture of the proposed neural circuit is built upon an essential biophysical assumption. Two capacitive elements, including a memcapacitor and a common capacitor, are combined in parallel via a linear resistor, and the coupled device describes the two-layer cell membrane with flexibility in the outer membrane. Additive branch circuits are incorporated with an inductor, a constant source, and a nonlinear resistor, and are suitable for measuring the electrical activities in the corresponding ion channels. In addition, one linear resistor in the inductive branch circuit is used to estimate the Joule heat during ion propagation in the ion channel. The linear resistor connecting two capacitive elements describes the material property between outer and inner cell membranes, and its consumption of Joule heat explains the filtering function of the cell membrane, when intracellular ions are pumped to pass through the ion channels embedded in the cell membrane. The outer cell membrane is sensitive to external stimuli, and shape deformation will induce changes in the membrane parameter in the presence of external electric excitation i_S.

Following Kirchhoff's law, the correlation for the physical variables in Fig. 1 is given by

$$\begin{cases} C\dfrac{\mathrm{d}V_C}{\mathrm{d}t}=\dfrac{V_{MC}-V_C}{R_1}-i_L-i_{NR}, \\ L\dfrac{\mathrm{d}i_L}{\mathrm{d}t}=V_C-E-R_0 i_L, \\ i_{MC}=-\dfrac{V_{MC}-V_C}{R_1}+i_S. \end{cases} \tag{1}$$

In the circuit representation, the linear resistor R_1 simulates the resistance of the medium between the two membrane layers. Here, V_C denotes the voltage across the capacitor, while V_{MC} represents the voltage across the memcapacitor. The circuit in Fig. 1 is designed to reflect key physical properties of cell membranes. The

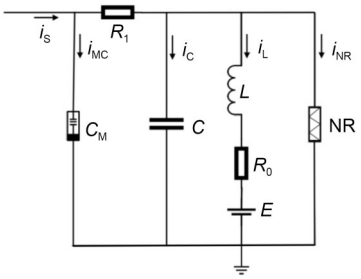

Fig. 1 Neural circuit with a memcapacitive membrane. *C*, *E*, C_M, *L*, and NR represent the capacitor, constant voltage power, memcapacitor, inductor, and nonlinear resistor, respectively

capacitor describes the capacitive behavior of the inner membrane due to static distribution and stochastic diffusion of intracellular ions and is assumed to have constant capacitance, meaning no changes in the inner membrane of the neuron. An inductor is introduced to simulate magnetic field effects induced by directional ionic currents across membrane channels. The nonlinear resistor captures the anisotropic coupling between electric and magnetic energy in complex intracellular environments. To account for the biophysical difference across membrane layers, a double-membrane structure is adopted: the inner membrane is modeled by a conventional capacitor, while the outer membrane—more susceptible to deformation under external stimuli—is represented by a memcapacitor with time-varying capacitance. This configuration enables simultaneous consideration of inner and outer membrane dynamics and their energy-dependent interactions. The channel current across the nonlinear resistor and the generalized memcapacitor are described by

$$\begin{cases} i_{NR}=-\dfrac{1}{\rho}\left(V_C-\dfrac{V_C^3}{3V_0^2}\right), \\ V_{MC}(t)=C_M^{-1}(\sigma)q(t), \\ \dfrac{\mathrm{d}q}{\mathrm{d}t}=i_{MC}, \\ \dfrac{\mathrm{d}\sigma}{\mathrm{d}t}=q. \end{cases} \tag{2}$$

Within this straight-line region, the current i_{NR} is proportional to the cross-voltage, and the resistivity remains a constant ρ. Here, V_0 represents the critical point where the i–V curve for the nonlinear resistor transitions from the linear region to the nonlinear region. The relationship between the inverse-capacitance of the memcapacitor (Han et al., 2024) used in this paper and the state variables is given by

$$C_M^{-1}(\sigma)=\frac{R_{12}}{R_{11}}\sigma+\frac{R_{12}}{R_{10}}\sigma^2. \tag{3}$$

The memcapacitor model derived from the equivalent circuit does not satisfy dimensional consistency, where the variable σ calculates charge accumulation within a transient period. The coefficients R_{12}/R_{11} and R_{12}/R_{10} have no physical units and therefore should be corrected by applying suitable physical parameters. To address this, two dimensional parameters are introduced: a with unit of $[1/(CTQ)]$ and b with unit of $[1/(CTQ)^2]$, where $[T]$ denotes time, $[C]$ denotes capacitance, and $[Q]$ denotes an electric charge unit (the square brackets "[ ]" denote the dimension of a physical

quantity). Accordingly, the inverse-capacitance expression of the memcapacitor is reformulated as follows:

$$C_{\mathrm{M}}^{-1}(\sigma)=a\frac{R_{12}}{R_{11}}\sigma+b\frac{R_{12}}{R_{10}}\sigma^2. \tag{4}$$

To describe the physical mechanism of the memcapacitor embedded in the proposed circuit, we consider its constitutive relation, in which the terminal voltage $V_{\mathrm{MC}}(t)$ is determined by the accumulated charge $q(t)$ and a state-dependent inverse-capacitance function $C_{\mathrm{M}}^{-1}(\sigma)$. The inverse capacitance is modeled as a quadratic function of the internal state variable $\sigma(t)$: $C_{\mathrm{M}}^{-1}(\sigma)=A_1\sigma+A_2\sigma^2$, where A_1 and A_2 are adjustable physical parameters associated with the properties of capacitance, resistance, and charge level. This nonlinear relationship implies that the memcapacitance $C_{\mathrm{M}}(\sigma)$ varies dynamically with the internal state, and the quadratic term introduces asymmetric modulation effects, distinguishing the device from conventional linear capacitors. The internal state σ evolves according to the time integral of charge, governed by $\mathrm{d}\sigma/\mathrm{d}t=q(t)$, which reflects the memory behavior intrinsic to the device, and its electrical properties depend not only on the instantaneous input but also on the entire history of charge flow. Under periodic excitation, this leads to the emergence of non-symmetric double-loop hysteresis in the q–V_{MC} characteristic, a hallmark of memcapacitive systems. The ratios R_{12}/R_{11} and R_{12}/R_{10} in Eq. (3) serve as tuning parameters that adjust the balance between linear and nonlinear contributions, enabling flexible modulation of the memory effect and mimicking biologically relevant membrane adaptation behaviors.

To facilitate subsequent analysis and simulation, all the involved variables have been updated in presenting dimensionless forms, resulting in a set of simplified control equations that describe the dynamic evolution process of the system, particularly focusing on the characteristic performance of the memcapacitor oscillator. The variables and physical parameters in Eqs. (1), (2), and (4) have been replaced by their equivalent dimensionless forms. The specific transformation criterion is given by

$$\begin{cases} x=\dfrac{V_{\mathrm{C}}}{V_0}, y=\dfrac{R_1 i_{\mathrm{L}}}{V_0}, z=\dfrac{q}{CV_0}, \\ w=\dfrac{\sigma}{C^2V_0R_1}, \tau=\dfrac{t}{R_1C}, I_{\mathrm{S}}=\dfrac{R_1 i_{\mathrm{S}}}{V_0}, \\ \lambda_1=\dfrac{R_1}{\rho}, \lambda_2=a\dfrac{R_{12}}{R_{11}}R_1C^3V_0, \\ \lambda_3=b\dfrac{R_{12}}{R_{10}}R_1^2C^5V_0^2, \lambda_4=\dfrac{R_1^2C}{L}, \\ \lambda_5=\dfrac{R_1R_0C}{L}, \lambda_6=\dfrac{R_1^2CE}{LV_0}. \end{cases} \tag{5}$$

The dynamics for the physical variables in Eq. (1) can be discussed in relation to the memcapacitor oscillator, which is given by

$$\begin{cases} \dfrac{\mathrm{d}x}{\mathrm{d}\tau}=(\lambda_1-1)x-\dfrac{1}{3}\lambda_1x^3-y+\lambda_2zw+\lambda_3zw^2, \\ \dfrac{\mathrm{d}y}{\mathrm{d}\tau}=\lambda_4x-\lambda_5y-\lambda_6, \\ \dfrac{\mathrm{d}z}{\mathrm{d}\tau}=x-\lambda_2zw-\lambda_3zw^2+I_{\mathrm{S}}, \\ \dfrac{\mathrm{d}w}{\mathrm{d}\tau}=z. \end{cases} \tag{6}$$

Physically, the memcapacitor defines a membrane whose permittivity changes based on the history of the electric field and stored charge, analogous to deformation or reconfiguration of lipid bilayers in response to sustained external stimulation. The resistor between the two capacitive layers reflects the intra-membrane resistance or dielectric coupling, capturing inter-layer ionic or structural interactions. The charge variable q governs the energy level and electric field in the memcapacitor, dictating how capacitance states evolve with stored charge. Within this neural circuit architecture, capacitors, the inductor, and the memcapacitor collectively store the field energy. During the scale transformation for physical time in Eq. (5), the reference time can also be selected as R_0C, and the dimensionless time scale $\tau=t/(R_0C)$ will support another group of new variables. The new theoretical model maintains the same physical and dynamical properties even though the obtained model may show some difference from Eq. (6). Consequently, the total field energy W and its corresponding dimensionless energy function H are defined by

$$\begin{cases} W=\dfrac{1}{2}CV^2+\dfrac{1}{2}Li_{\mathrm{L}}^2+\dfrac{1}{2}C_{\mathrm{M}}V_{\mathrm{MC}}^2 \\ \quad =CV_0^2\left(\dfrac{1}{2}x^2+\dfrac{1}{2\lambda_4}y^2+\dfrac{1}{2}\lambda_2wz^2+\lambda_3w^2z^2\right), \\ H=\dfrac{W}{CV_0^2}=\dfrac{1}{2}x^2+\dfrac{1}{2\lambda_4}y^2+\dfrac{1}{2}\lambda_2wz^2+\lambda_3w^2z^2, \\ H_{\mathrm{C}}=\dfrac{1}{2}x^2, H_{\mathrm{L}}=\dfrac{1}{2\lambda_4}y^2, \\ H_{\mathrm{MC}}=\dfrac{1}{2}\lambda_2wz^2+\lambda_3w^2z^2. \end{cases} \tag{7}$$

The field energy of the neural circuit is saved in these electric components, and its equivalent dimensionless form H can be derived by recasting the neuron model presented in Eq. (6) into an equivalent vector representation, leveraging the Helmholtz decomposition criterion.

$$\begin{cases} \dfrac{\mathrm{d}\boldsymbol{X}}{\mathrm{d}\tau}=\boldsymbol{F}_{\mathrm{c}}(x,y,z)+\boldsymbol{F}_{\mathrm{d}}(x,y,z) \\ \quad =\left[J(x,y,z)+R(x,y,z)\right]\nabla H, \\ (\nabla H)^{\mathrm{T}}\boldsymbol{F}_{\mathrm{c}}(x,y,z)=0, \\ (\nabla H)^{\mathrm{T}}\boldsymbol{F}_{\mathrm{d}}(x,y,z)=\dfrac{\mathrm{d}H}{\mathrm{d}\tau}, \end{cases} \tag{8}$$

where the gradient energy ∇H describes the gradient distribution of spatial forces, the skew-symmetric matrix $\boldsymbol{J}(\boldsymbol{X})$ represents the vortex field $\boldsymbol{F}_{\mathrm{c}}(\boldsymbol{X})$, and the symmetric matrix $\boldsymbol{R}(\boldsymbol{X})$ relates to the gradient field $\boldsymbol{F}_{\mathrm{d}}(\boldsymbol{X})$. Following the criterion in Eq. (8), the neuron with memcapacitive variable and two-layer membranes can be expressed by Eq. (9).

$$\begin{aligned}\begin{bmatrix}\dot{x}\\ \dot{y}\\ \dot{z}\\ \dot{w}\end{bmatrix}&=\begin{bmatrix}(\lambda_1-1)x+\lambda_2 zw+\lambda_3 zw^2-y-\frac{1}{3}\lambda_1 x^3\\ \lambda_4 x-\lambda_5 y-\lambda_6\\ x-\lambda_2 zw-\lambda_3 zw^2+I_S\\ z\end{bmatrix}\\&=\begin{bmatrix}\lambda_2 zw+\lambda_3 zw^2-y\\ \lambda_4 x\\ -x\\ 0\end{bmatrix}+\begin{bmatrix}(\lambda_1-1)x-\frac{1}{3}\lambda_1 x^3\\ -\lambda_5 y-\lambda_6\\ 2x-\lambda_2 zw-\lambda_3 zw^2+I_S\\ z\end{bmatrix}\\&=\begin{bmatrix}0&-\lambda_4&1&0\\ \lambda_4&0&0&0\\ -1&0&0&0\\ 0&0&0&0\end{bmatrix}\begin{bmatrix}x\\ \frac{y}{\lambda_4}\\ \lambda_2 zw+\lambda_3 zw^2\\ 0.5\lambda_2 z^2+\lambda_3 z^2 w\end{bmatrix}\\&+\begin{bmatrix}a_{11}&0&0&0\\ 0&a_{22}&0&0\\ 0&0&a_{33}&0\\ 0&0&0&a_{44}\end{bmatrix}\begin{bmatrix}x\\ \frac{y}{\lambda_4}\\ \lambda_2 zw+\lambda_3 zw^2\\ 0.5\lambda_2 z^2+\lambda_3 z^2 w\end{bmatrix},\end{aligned}\tag{9}$$

where

$$a_{11}=(\lambda_1-1)-\frac{1}{3}\lambda_1 x^2,\ a_{22}=\frac{(-\lambda_5 y-\lambda_6)\lambda_4}{y},$$
$$a_{33}=\frac{2x-\lambda_2 zw-\lambda_3 zw^2+I_S}{\lambda_2 zw+\lambda_3 zw^2},\ a_{44}=\frac{1}{0.5\lambda_2 z+\lambda_3 zw}.$$

Notably, the eigenvector in Eq. (9) is consistent with the gradient energy term specified in Eq. (7). Thus, the neuron model developed from the neural circuit has a unique and exact energy function. Variations in energy levels can influence the firing behavior and membrane potential. On the other hand, alterations in intrinsic parameters or membrane potential can indicate potential shifts in the neuron's energy state. The introduction of external forcing injects energy into the system, thereby triggering dynamic changes in the memcapacitive membrane, and then the energy proportion of other branch circuits/ion channels is changed synchronously. As a result, one of the coherent parameters with the memcapacitor (λ_2, λ_3) can be regarded as a tunable parameter, whose evolution is regulated by the energy flow within the system.

$$\begin{aligned}&\frac{\mathrm{d}\lambda_3}{\mathrm{d}\tau}=\sigma\lambda_3\Theta(H-\lambda),\\&\Theta(P)=\begin{cases}1, P\geq 0,\\ 0, P<0.\end{cases}\end{aligned}\tag{10}$$

Here, $\Theta(P)$ denotes the Heaviside step function. Specifically, the gain parameter σ determines the step size of memcapacitance growth, and the parameter for the higher-order term of memcapacitance begins to increase exponentially when the system energy exceeds a certain threshold λ. To probe the influence of external fields on the capacitor channel and memcapacitor, zero-mean Gaussian white noise (statistical property$<S_{ext}(\tau)$, $S_{ext}(\tau')\geq D\delta(\tau-\tau')$) with intensity D can be incorporated into the first and third terms of Eq. (6). The additive noisy excitations result from stochastic fluctuation in the electric field. This stochastic perturbation enables investigation of noise-driven stochastic phenomena in individual neurons via controlled intensity modulation.

The coefficient of variation CV predicts the correlation and regularity of the sampled time series for signal series and is considered a statistical approach suitable for use on available sampled time series for one variable in the system. The noise intensity is changed carefully to detect the appearance of the lowest CV value, and coherence/stochastic resonance is induced and predicted, which is shown as

$$\mathrm{CV}=\frac{\sqrt{<T^2>-<T>^2}}{<T>},\tag{11}$$

where $\Delta\tau=T$ denotes the inter-spike interval (ISI) of the membrane potential time series and serves as a measure of temporal regularity. Simultaneously, the average value of energy $<H>$ is computed via

$$<H>=\frac{1}{\tau}\int_0^{\tau}H(\tau)\mathrm{d}\tau\approx\frac{1}{N}\sum_{i=1}^{N}H_i.\tag{12}$$

Within a transient period, $t=Nh$ is used to find numerical solutions, where N indicates the number of iterations and h is the time step for numerical simulation. Analysis reveals stochastic resonance at the specific noise intensity where the CV versus noise intensity curve attains its global minimum. Concurrently, the $<H>$ versus noise intensity profile reaches its peak at this identical intensity, corroborating the resonance condition. Bifurcation analysis and coherence resonance are described in the following section, followed by the implementation of an adaptive control scheme to modulate energy levels and govern transitions in neural firing patterns.

3 Numerical results and discussions

Modifying component physical parameters or external excitation intensity in neural circuits can induce voltage output patterns resembling biological neuronal firings. The external stimuli applied in the model take the form of a periodic signal, specifically $I_S=A\cos(\omega\tau)$, representing rhythmic environmental inputs, where A is the amplitude and ω is the angular frequency. The fourth-order Runge–Kutta method is used to find the time series of variables for further nonlinear analysis. Numerical simulations herein use a dimensionless integration step size of h=0.01.

Bifurcation analysis serves as an effective tool for predicting transitions in neuronal firing patterns. Peak values of the membrane potential (x_{peak}) are extracted from the time series in the presence of varying parameters under the external driving signal. Here, x_{peak} refers to the maximum amplitude observed in the sampled neuronal membrane potential. By adjusting the memcapacitive parameters λ_2 and λ_3, the neuron exhibits transitions between periodic and chaotic dynamics. These switches are captured through variations in peak values of the membrane potential, with the largest Lyapunov exponent (LLE) plotted against different values of λ_2 and λ_3 (Fig. 2).

The results in Fig. 2 indicate that chaotic behavior can emerge within specific parameter ranges. However, as the bifurcation

parameters continue to increase, the system eventually settles into a stable regime characterized by a negative LLE and the suppression of chaotic oscillations, as shown by the extensive numerical results in Fig. 3.

The neuron described by Eq. (6) can exhibit bursting, spiking, or chaotic activities when the angular frequency or amplitude of the external stimuli is carefully tamed (Fig. 3). To simplify the analysis, different amplitudes and angular frequencies are applied to induce distinct firing behaviors, and the associated energy levels are computed. Figs. 4 and 5 present the phase portraits corresponding to chaotic, bursting, and periodical states and the evolution of the system's energy.

When chaotic activity in the neuron is suppressed, giving rise to bursting or periodic firing modes, the underlying attractors are reshaped, accompanied by a notable change in the average energy level. Typically, the chaotic state is associated with a lower average energy value. As plotted in Eq. (7), the total energy function comprises three components: capacitive, inductive, and memcapacitive energy terms. To better understand their respective roles, Fig. 6 presents the relative contributions of each component to the average energy, allowing for a more detailed interpretation of how energy is redistributed during dynamic transitions.

The memcapacitive term contributes most of the total Hamilton energy, often exceeding the combined contributions from the

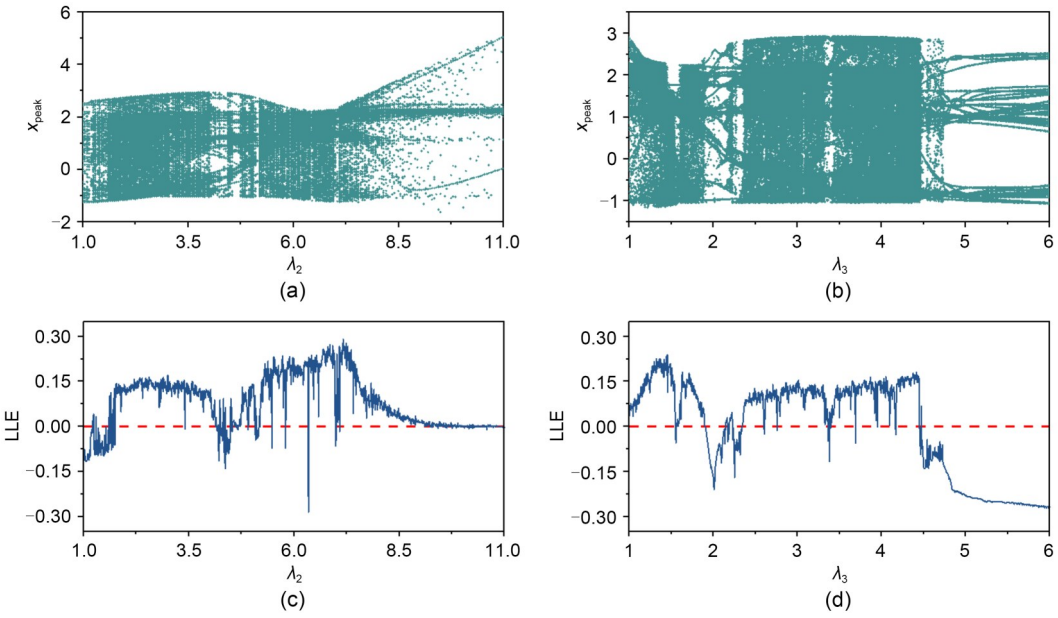

Fig. 2 Distribution of peak values of the membrane potential (a and b) and LLE (c and d) versus bifurcation parameters. λ_3=3.8 for (a) and (c), and λ_2=3.3 for (b) and (d). λ_1=1.8, λ_4=2.8, λ_5=6, λ_6=0.05, A=5.8, ω=2, and initial conditions are fixed at (2, 2, 0.1, 0.1)

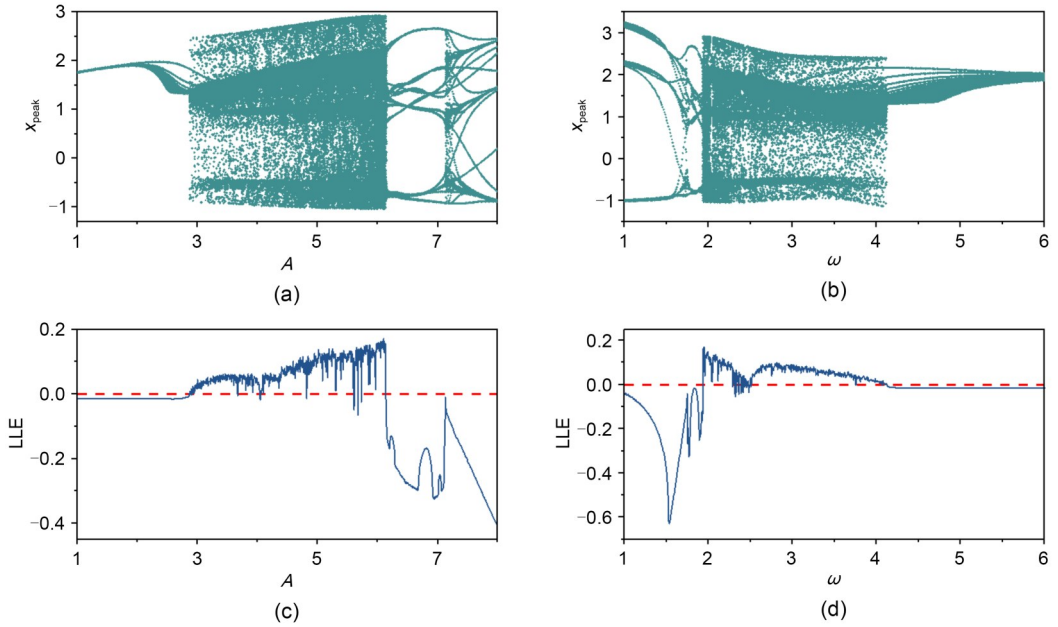

Fig. 3 Distribution of peak values of the membrane potential (a and b) and LLE (c and d) versus bifurcation parameters. ω=2 for (a) and (c), and A=5.8 for (b) and (d). λ_1=1.8, λ_2=3.3, λ_3=3.8, λ_4=2.8, λ_5=6, λ_6=0.05, and initial conditions are fixed at (2, 2, 0.1, 0.1)

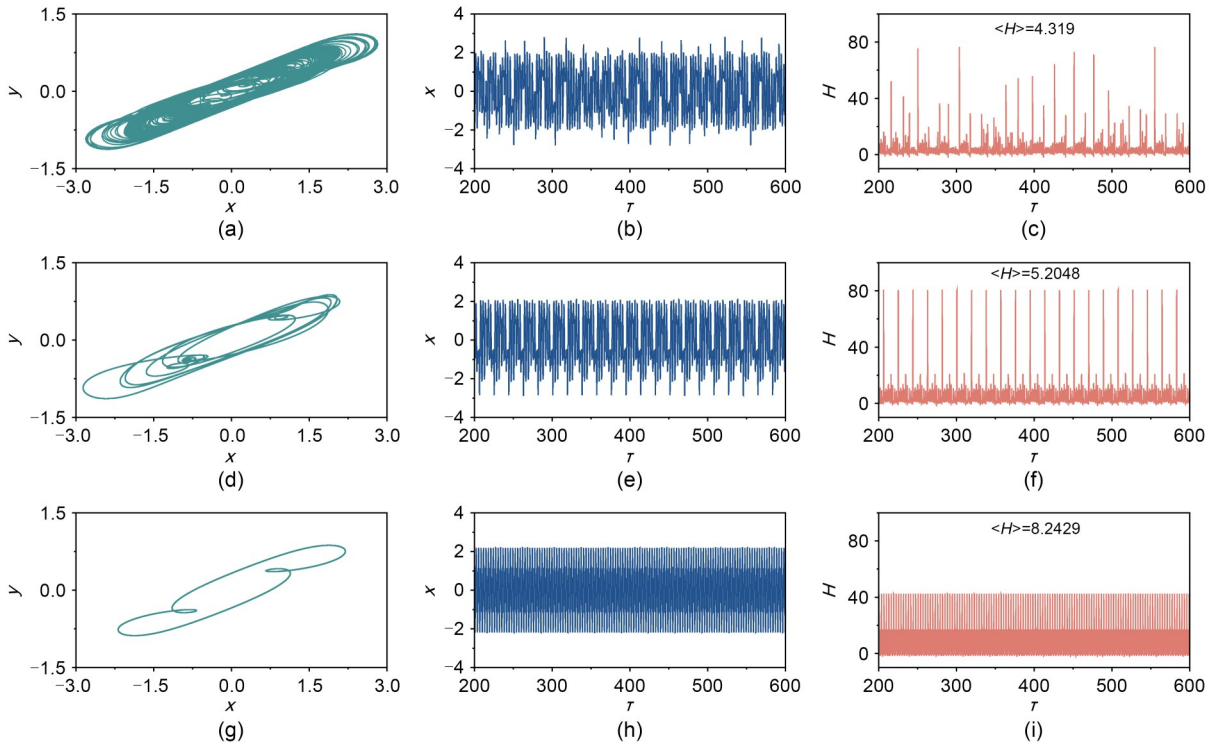

Fig. 4 Phase portraits (a, d, g) and evolution of membrane potential (b, e, h) and energy value (c, f, i) corresponding to chaotic (a–c, A=5.2), bursting (d–f, A=5.608), and periodical (g–i, A=7.5) states. λ_1=1.8, λ_2=3.3, λ_3=3.8, λ_4=2.8, λ_5=6, λ_6=0.05, ω=2, and initial conditions are fixed at (2, 2, 0.1, 0.1)

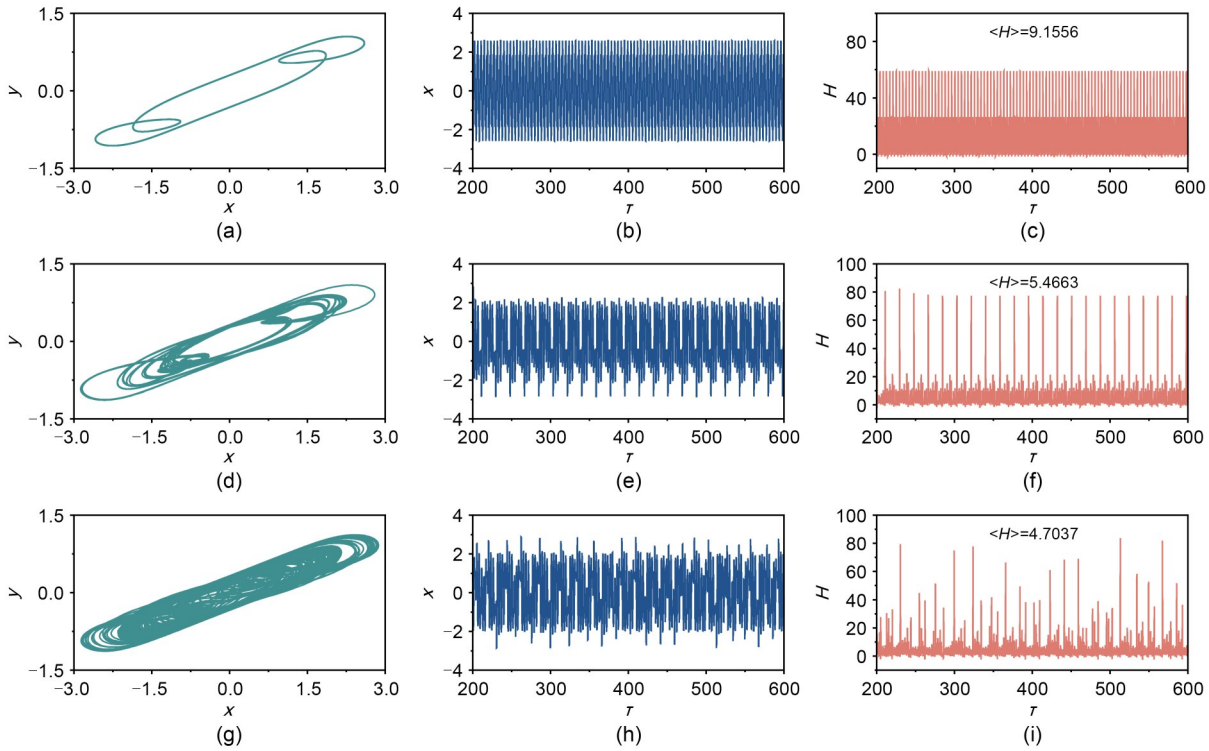

Fig. 5 Phase portraits (a, d, g) and evolution of membrane potential (b, e, h) and energy value (c, f, i) corresponding to periodical (a–c, ω=1.5), bursting (d–f, ω=2.045), and chaotic (g–i, ω=2.09) states. λ_1=1.8, λ_2=3.3, λ_3=3.8, λ_4=2.8, λ_5=6, λ_6=0.05, A=5.8, and initial conditions are fixed at (2, 2, 0.1, 0.1)

capacitive and inductive elements (Fig. 6). This underscores its regulatory dominance in determining firing patterns and energy flow within the neuron. The capacitive and inductive energy components contribute significantly less, with negligible fluctuations in presenting different firing modes. Crucially, the memcapacitor strongly influences the neuron's firing patterns: chaotic firing correlates with reduced memcapacitive energy storage, whereas periodic firing coincides with peak memcapacitive energy levels. The dynamic behavior of the neuron under the influence of the adaptive regulation described in Eq. (10) is worthy of investigation, especially in terms

of mode transitions and associated energy variations. The results are illustrated in Fig. 7.

Counterintuitively, implementing a larger gain increases the transient period for reaching the saturation value for the growing parameter λ_3 because the dynamics of firing patterns is dependent on this parameter in a nonlinear way. This firing pattern transition corresponds with energy variations, leading to stable periodic firing modes.

To evaluate and confirm the stochastic characteristics and effects, Gaussian white noise is incorporated into the neuron for regulating neural activities. We characterize the response by computing the dependence on the noise intensity D of both the coefficient of variation CV and the average value of energy $<H>$. Fig. 8 illustrates the dependence of CV and $<H>$ on noise intensity D under two distinct perturbation schemes: introducing noise into the membrane potential equation (i.e., the first state variable); introducing noise into the memcapacitor channel dynamics (i.e., the third state variable).

When noise is applied to the first or third term of Eq. (6), it represents the impact of external electric field fluctuations on the capacitor channel and the memcapacitor channel, respectively. When applying Gaussian white noise perturbations, both cases exhibit stochastic resonance phenomena. When noise is applied to the memcapacitor channel (outer membrane), the CV value at resonance is lower (0.187 64), while the corresponding $<H>$ is higher (5.236 44). This indicates the occurrence of stronger resonance intensity, higher rhythmic firing regularity, and enhanced coherence compared to the resonant state observed when noise is applied to the capacitive channel (inner membrane). The emergence of stochastic resonance requires different thresholds when noise is applied to regulate the outer and inner membranes. Similarly, stochastic resonance can be induced when additive noise is imposed for exciting the second variable for the inductive channel, and the mean energy obtains another maximum value at moderate noise intensity. To validate the dynamic characteristics governed by Eq. (6), an analog circuit composed of operational amplifiers, analog multipliers, resistors, and capacitors is constructed (Fig. 9). The corresponding firing patterns under different input amplitudes are presented in Fig. 10.

During the operation of the analog neural circuit, its firing dynamics can be controlled by varying the external voltage input. By modulating the stimulus amplitude, the circuit exhibits both periodic and chaotic behaviors. This circuit implementation strengthens the practical relevance of the proposed model, with the simulated outcomes in Fig. 10 showing excellent agreement with the numerical results shown in Figs. 4a, 4b, 4g, and 4h.

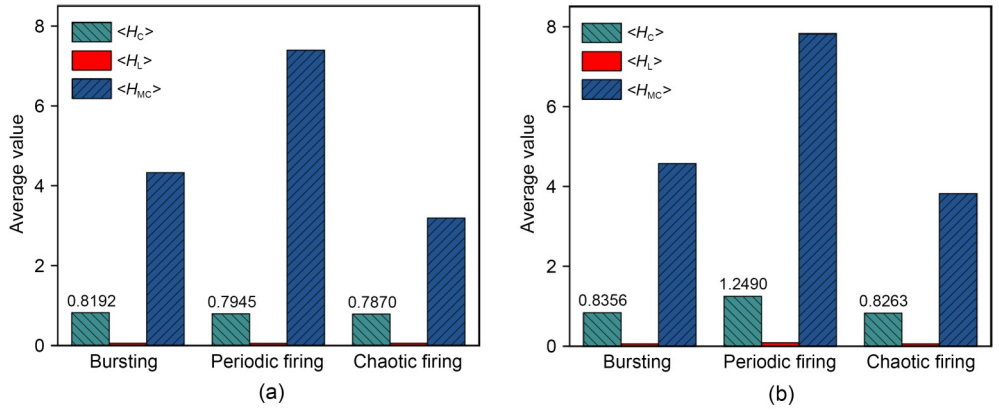

Fig. 6 Average values for capacitive, inductive, and memcapacitive energy terms: (a) ω=2, bursting A=5.608, periodic firing A=7.5, chaotic firing A=5.2; (b) A=5.8, bursting ω=2.045, periodic firing ω=1.5, chaotic firing ω=2.09. λ_1=1.8, λ_2=3.3, λ_4=2.8, λ_5=6, λ_6=0.05, and initial conditions are fixed at (2, 2, 0.1, 0.1)

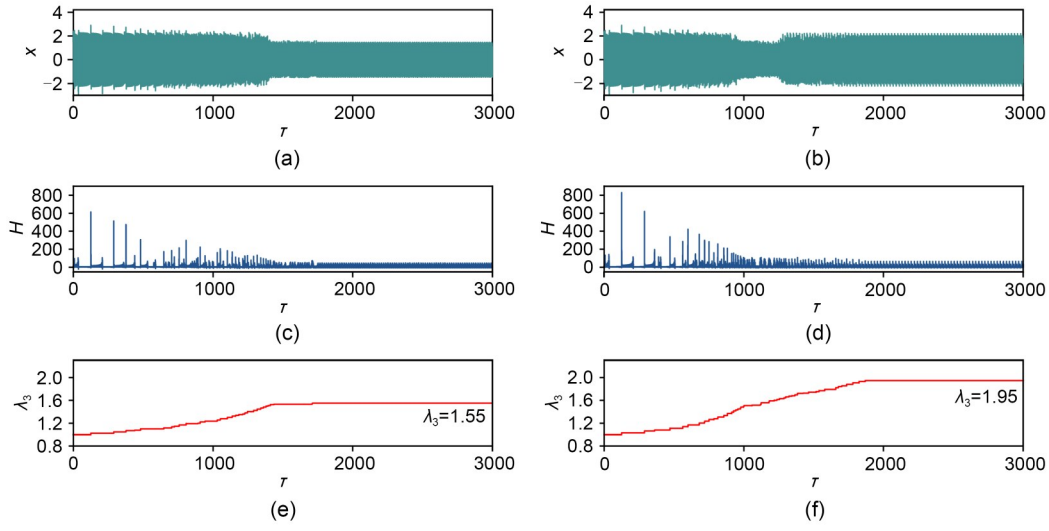

Fig. 7 Evolution of firing patterns (a and b), energy levels (c and d), and parameters (e and f) under the adaptive control law. σ=0.06 for (a–c), and σ=0.08 for (d–f). λ_1=1.8, λ_2=3.3, λ_4=2.8, λ_5=6, λ_6=0.05, A=5.8, ω=2, λ=65, and initial conditions are fixed at (2, 2, 0.1, 0.1). The parameter λ_3 begins its growth from 1

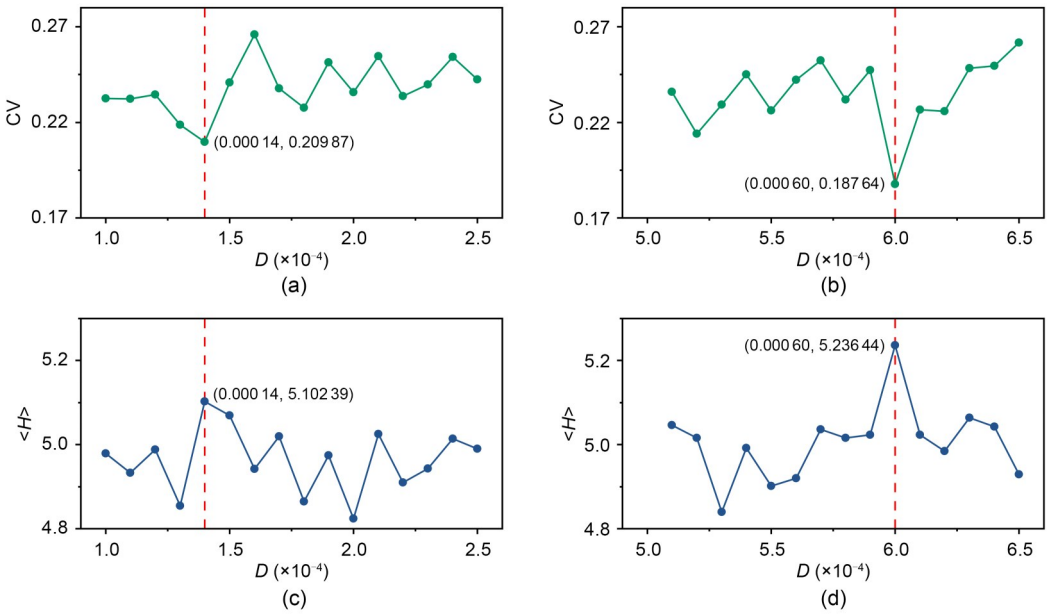

Fig. 8 Dependence of CV and <*H*> on noise intensity *D* under two distinct perturbation schemes: (a, c) the noisy excitation is applied to the right side of the first formula in Eq. (6); (b, d) the noisy excitation is applied to the right side of the third formula in Eq. (6). λ_1=1.8, λ_2=3.3, λ_3=3.8, λ_4=2.8, λ_5=6, λ_6=0.05, A=5.8, ω=2, and initial conditions are fixed at (2, 2, 0.1, 0.1)

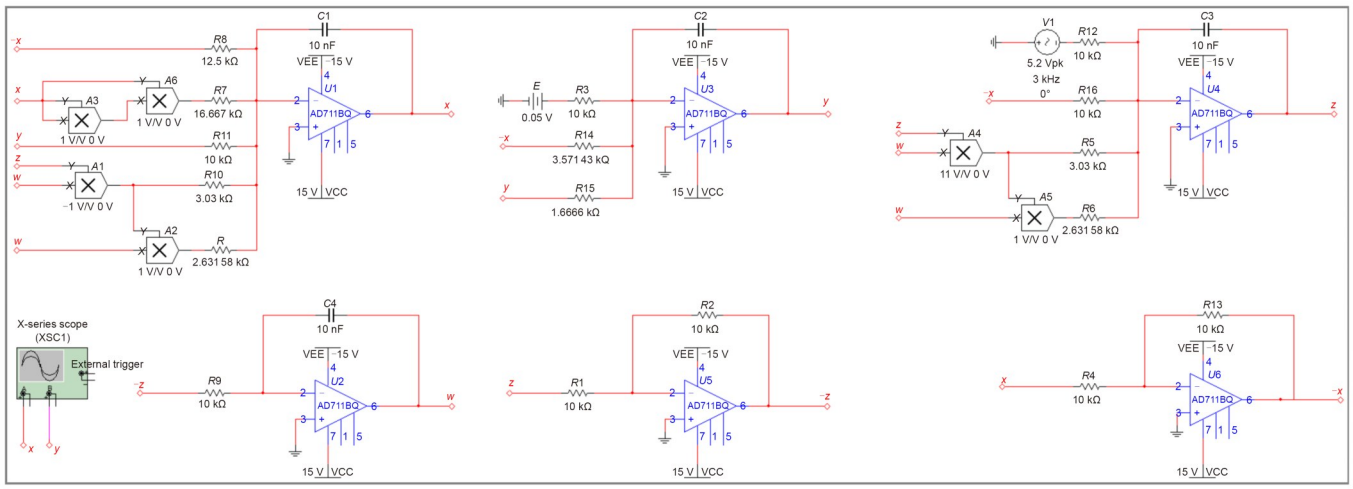

Fig. 9 Analog circuit implementation based on Multisim. An external voltage V_1 is imposed on the working unit. VEE: emitter voltage; VCC: voltage collector common

In summary, the numerical analysis confirms that the proposed memcapacitive neuron model exhibits diverse dynamical behaviors, including chaotic, bursting, and periodic firing, under various parameter regimes. The memcapacitor plays a decisive role in modulating these behaviors through its energy-dependent properties. The inclusion of adaptive control and stochastic perturbations further enhances the model's flexibility, allowing for energy-guided transitions and coherence optimization. Indeed, incorporation of the memcapacitor into the neural circuit is well suited for measuring the flexible property of the cell membrane, and the effect of shape deformation of the outer membrane of the neuron is estimated in a quantitative way. Importantly, experimental implementation using analog circuits validates the theoretical predictions and demonstrates the physical feasibility of the model, thereby reinforcing its relevance in bio-inspired neuromorphic systems. That is, by considering the main physical properties of biological neurons, distinct resonance characteristics under noisy excitation can be induced by our proposed model. Besides the common stochastic resonance, the occurrence of similar inverse stochastic resonance (ISR) (Lu et al., 2020; Zamani et al., 2020; Wang XQ et al., 2023; Yamakou et al., 2024) can be discussed. This study aims to investigate an approach to modeling a single neuron with a controllable memory cell membrane. The theoretical model can be further used to explore the collective dynamics, including synchronization stability and pattern formation in networks composed of the same neurons or neurons with parameter diversity. In addition, memristors can be connected to additive branch circuits of the neural circuit, and the memristive channel becomes controllable in signal processing. For further biophysical guidance and potential application of similar neural circuits, readers are referred to recent reviews and references therein (Ma and Guo, 2024; Ma, 2025).

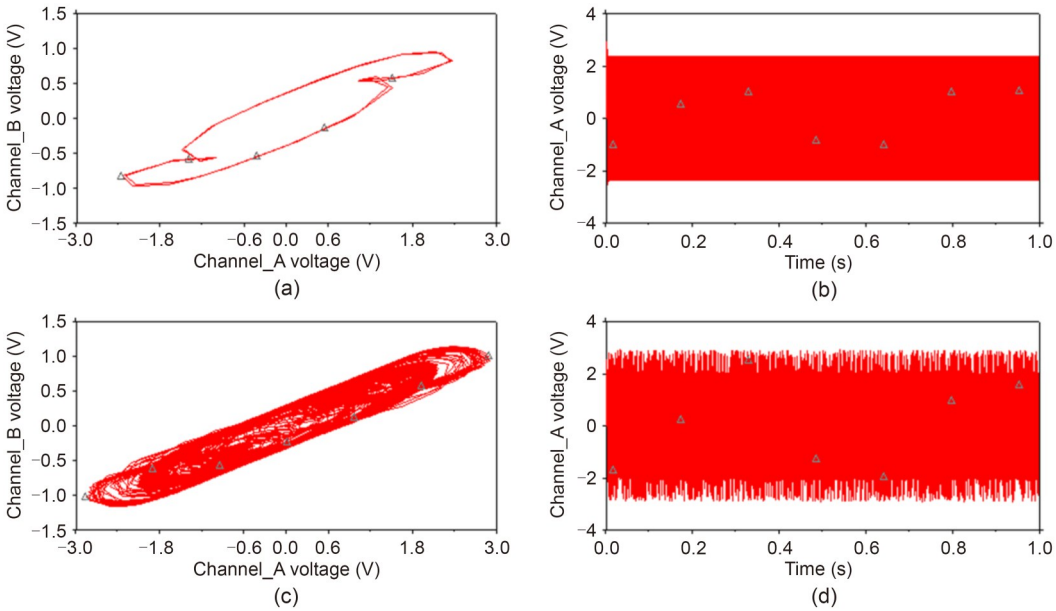

Fig. 10 Phase portraits (a, c) and evolution of output voltage of circuit simulation with different amplitudes (b, d) in external stimuli V_1. V_1=7.5 V (a and b) and V_1=5.2 V (c and d), corresponding to the periodic firing pattern and the chaotic firing pattern, respectively

4 Conclusions

In this study, an additional memcapacitor is integrated into the FHN neural circuit and connected to a traditional capacitor via a linear resistor to simulate both the capacitive properties and deformation characteristics of a cell membrane. This configuration enables the characterization of capacitive energy diversity in neurons with memcapacitive membranes and allows the controllability of the membrane to be described by adjusting the memcapacitance parameters. The proposed neuron can be considered a new model containing two capacitive variables, and the physical mechanism of capacitance regulation is explained. That is, both external electric stimuli and electric field polarization modify the energy levels of the neuron, and the outer cell membrane regulates its capacitance based on the charge levels and energy value. Under external stimulation, changes in energy levels and distribution are observed, and the memcapacitive neuron exhibits transitions in firing modes. By modulating the noise intensity, stochastic resonance can be induced, leading to highly regular neural activity at an optimal noise level, which also supports the maintenance of maximum Hamilton energy. In this paper, we propose a novel memcapacitor-based neuron model with improved biophysical relevance, as it incorporates additional physical effects to better emulate the behaviors of real biological neurons. Although this study focuses on a single-neuron model, future studies could extend it to network-level investigations. The memcapacitive neuron model not only enriches theoretical understanding but also points to potential applications. Its adaptive capacitive property and the observed stochastic resonance effect suggest prospects in reconfigurable neuromorphic hardware and noise-tolerant neural signal processing.

Acknowledgments

This work was supported by the National Natural Science Foundation of China (No. 12072139).

Author contributions

Binchi WANG and Yitong GUO completed model description, formal analysis, and numerical calculation. Guodong REN presented formal analysis and circuit verification. Jun MA suggested this investigation and drafted, revised, and finalized the paper.

Conflict of interest

All the authors declare that they have no conflict of interest.

Data availability

The data that support the findings of this study are available from the corresponding author upon reasonable request.

Declaration on the use of generative AI tools

During the preparation of this work, the authors used ChatGPT in order to improve language. After using this tool, the authors reviewed and edited the content as needed and take full responsibility for the content of the published article.

References

Beilliard Y, Alibart F, 2021. Multi-terminal memristive devices enabling tunable synaptic plasticity in neuromorphic hardware: a mini-review. *Front Nanotechnol*, 3: 779070. https://doi.org/10.3389/fnano.2021.779070

Budhathoki RK, Sah MP, Adhikari SP, et al., 2013. Composite behavior of multiple memristor circuits. *IEEE Trans Circ Syst I Regul Pap*, 60(10):2688-2700. https://doi.org/10.1109/TCSI.2013.2244320

Bullmore E, Sporns O, 2009. Complex brain networks: graph theoretical analysis of structural and functional systems. *Nat Rev Neurosci*, 10(3):186-198. https://doi.org/10.1038/nrn2575

Busygin AN, Pisarev AD, Udovichenko SY, et al., 2025. Memory device based on memristor-diode crossbar and control CMOS logic for spiking neural network hardware. *Integration*, 104:102461. https://doi.org/10.1016/j.vlsi.2025.102461

Cebrián-Lacasa D, Parra-Rivas P, Ruiz-Reynés D, et al., 2024. Six decades of the FitzHugh–Nagumo model: a guide through its spatio-temporal dynamics and influence across disciplines. *Phys Rep*, 1096:1-39. https://doi.org/10.1016/j.physrep.2024.09.014

Chen YX, Mou J, Jahanshahi H, et al., 2023. A new mix chaotic circuit based on memristor–memcapacitor. *Eur Phys J Plus*, 138(1):78. https://doi.org/10.1140/epjp/s13360-023-03699-7

Deswal S, Kumar A, Kumar A, 2019. NbOx based memristor as artificial synapse emulating short term plasticity. *AIP Adv*, 9(9):095022.

https://doi.org/10.1063/1.5118980

Di Ventra M, Pershin YV, Chua LO, 2009. Circuit elements with memory: memristors, memcapacitors, and meminductors. *Proc IEEE*, 97(10):1717-1724. https://doi.org/10.1109/JPROC.2009.2021077

Dong ZK, Lai CS, Zhang ZW, et al., 2021. Neuromorphic extreme learning machines with bimodal memristive synapses. *Neurocomputing*, 453:38-49. https://doi.org/10.1016/j.neucom.2021.04.049

FitzHugh R, 1961. Impulses and physiological states in theoretical models of nerve membrane. *Biophys J*, 1(6):445-466. https://doi.org/10.1016/S0006-3495(61)86902-6

Ge MY, Jia K, Gao RY, et al., 2025a. Neural behaviors and energy properties of memcapacitor FitzHugh–Nagumo neuron model with Miller effect. *Nonl Dyn*, 113(3):2689-2710. https://doi.org/10.1007/s11071-024-10349-9

Ge MY, Jia K, Wang X, et al., 2025b. Researches on dynamics and noise effects of FHN neuron based on memristor–memcapacitor coupling. *Nonl Dyn*, 113(19): 26671-26693. https://doi.org/10.1007/s11071-025-11454-z

Gerster M, Berner R, Sawicki J, et al., 2020. FitzHugh–Nagumo oscillators on complex networks mimic epileptic-seizure-related synchronization phenomena. *Chaos*, 30(12):123130. https://doi.org/10.1063/5.0021420

Guo YT, Wu FQ, Yang FF, et al., 2023. Physical approach of a neuron model with memristive membranes. *Chaos*, 33(11):113106. https://doi.org/10.1063/5.0170121

Guo YT, Ma J, Zhang XF, et al., 2024. Memristive oscillator to memristive map, energy characteristic. *Sci China Technol Sci*, 67(5):1567-1578. https://doi.org/10.1007/s11431-023-2637-1

Han ZT, Al-Barakati AA, Jahanshahi H, et al., 2024. A novel circuit based on memristor–memcapacitor with extreme multistability. *Nonl Dyn*, 112(6):4863-4877. https://doi.org/10.1007/s11071-024-09286-4

Herculano-Houzel S, 2009. The human brain in numbers: a linearly scaled-up primate brain. *Front Hum Neurosci*, 3:31. https://doi.org/10.3389/neuro.09.031.2009

Huang W, Xia XW, Zhu C, et al., 2021. Memristive artificial synapses for neuromorphic computing. *Nano-Micro Lett*, 13(1):85. https://doi.org/10.1007/s40820-021-00618-2

Indiveri G, Linares-Barranco B, Legenstein R, et al., 2013. Integration of nanoscale memristor synapses in neuromorphic computing architectures. *Nanotechnology*, 24(38):384010. https://doi.org/10.1088/0957-4484/24/38/384010

Isah A, Bilbault JM, 2022. Review on the basic circuit elements and memristor interpretation: analysis, technology and applications. *J Low Power Electron Appl*, 12(3): 44. https://doi.org/10.3390/jlpea12030044

Ji YS, Mao XC, 2024. Spatiotemporal dynamics of a modified FitzHugh–Nagumo neuronal network with time delays. *Nonl Dyn*, 112(9):7571-7582. https://doi.org/10.1007/s11071-024-09424-y

Khacef L, Klein P, Cartiglia M, et al., 2023. Spike-based local synaptic plasticity: a survey of computational models and neuromorphic circuits. *Neuromorph Comput Eng*, 3(4):042001. https://doi.org/10.1088/2634-4386/ad05da

Lei Z, Guo YT, Ma J, et al., 2025. Physical characteristic and dynamics in a neural circuit without using inductor and nonlinear resistor. *Chaos Sol Fract*, 199(part 1): 116735. https://doi.org/10.1016/j.chaos.2025.116735

Li JY, Abbas H, Ang DS, et al., 2023. Emerging memristive artificial neuron and synapse devices for the neuromorphic electronics era. *Nanoscale Horiz*, 8(11):1456-1484. https://doi.org/10.1039/D3NH00180F

Li PY, Li ZJ, 2025. Hidden electrical activities in a memcapacitor-based FitzHugh–Nagumo circuit. *Eur Phys J Spec Top*, early access. https://doi.org/10.1140/epjs/s11734-025-01727-4

Li Y, Shen GZ, 2022. Advances in optoelectronic artificial synapses. *Cell Rep Phys Sci*, 3(9):101037. https://doi.org/10.1016/j.xcrp.2022.101037

Li YN, Ma J, Xie Y, 2024a. A biophysical neuron model with double membranes. *Nonl Dyn*, 112(9):7459-7475. https://doi.org/10.1007/s11071-024-09452-8

Li YN, Lv M, Ma J, et al., 2024b. A discrete memristive neuron and its adaptive dynamics. *Nonl Dyn*, 112(9):7541-7553. https://doi.org/10.1007/s11071-024-09361-w

Lu LL, Jia Y, Ge MY, et al., 2020. Inverse stochastic resonance in Hodgkin–Huxley neural system driven by Gaussian and non-Gaussian colored noises. *Nonl Dyn*, 100(1):877-889. https://doi.org/10.1007/s11071-020-05492-y

Ma J, 2023. Biophysical neurons, energy, and synapse controllability: a review. *J Zhejiang Univ Sci A*, 24(2):109-129. https://doi.org/10.1631/jzus.A2200469

Ma J, 2025. Biological neurons to neural circuit, review from physical perspective. *Nonl Dyn*, 113(19):25365-25387. https://doi.org/10.1007/s11071-025-11487-4

Ma J, Guo YT, 2024. Model approach of electromechanical arm interacted with neural circuit, a minireview. *Chaos Sol Fract*, 183:114925. https://doi.org/10.1016/j.chaos.2024.114925

Minati L, Gambuzza LV, Thio WJ, et al., 2020. A chaotic circuit based on a physical memristor. *Chaos Sol Fract*, 138:109990. https://doi.org/10.1016/j.chaos.2020.109990

Panda S, Dash CS, Dora C, 2024. Recent trends in application of memristor in neuromorphic computing: a review. *Curr Nanosci*, 20(4):495-509. https://doi.org/10.2174/1573413719666230516151142

Plotnikov SA, Fradkov AL, 2016. Controlled synchronization in two hybrid FitzHugh–Nagumo systems. *IFAC-PapersOnLine*, 49(14):137-141. https://doi.org/10.1016/j.ifacol.2016.07.998

Plotnikov SA, Fradkov AL, 2019. On synchronization in heterogeneous FitzHugh–Nagumo networks. *Chaos Sol Fract*, 121:85-91. https://doi.org/10.1016/j.chaos.2019.02.006

Prezioso M, Merrikh-Bayat F, Hoskins BD, et al., 2015. Training and operation of an integrated neuromorphic network based on metal-oxide memristors. *Nature*, 521(7550):61-64. https://doi.org/10.1038/nature14441

Prezioso M, Merrikh Bayat F, Hoskins B, et al., 2016. Self-adaptive spike-time-dependent plasticity of metal-oxide memristors. *Sci Rep*, 6:21331. https://doi.org/10.1038/srep21331

Quininao C, Touboul JD, 2020. Clamping and synchronization in the strongly coupled FitzHugh–Nagumo model. *SIAM J Appl Dyn Syst*, 19(2):788-827. https://doi.org/10.1137/19M1283884

Romero FJ, Ohata A, Toral-Lopez A, et al., 2021. Memcapacitor and meminductor circuit emulators: a review. *Electronics*, 10(11):1225. https://doi.org/10.3390/electronics10111225

Scialla S, Loppini A, Patriarca M, et al., 2021. Hubs, diversity, and synchronization in FitzHugh–Nagumo oscillator networks: resonance effects and biophysical implications. *Phys Rev E*, 103(5):052211. https://doi.org/10.1103/PhysRevE.103.052211

Shao Y, Wu FQ, Wang QY, 2024. Synchronization and complex dynamics in locally active threshold memristive neurons with chemical synapses. *Nonl Dyn*, 112(15): 13483-13502. https://doi.org/10.1007/s11071-024-09747-w

Shao Y, Wu FQ, Wang QY, 2025. Excitability and synchronization of vanadium dioxide memristor-inspired neurons. *Math Comput Simul*, 233:99-116. https://doi.org/10.1016/j.matcom.2025.01.022

Shi F, Cao YH, Banerjee S, et al., 2024. A novel neural networks with memristor coupled memcapacitor-synapse neuron. *Chaos Sol Fract*, 189(part 2):115723. https://doi.org/10.1016/j.chaos.2024.115723

Song XL, Yang FF, 2025. Analysis of electrical activities in a functional neuron with dual memristors. *J Theor Biol*, 599:112034. https://doi.org/10.1016/j.jtbi.2024.112034

Song XL, Wang Y, Yang FF, 2025. A map neuron with a hybrid ion channel and its dynamics. *Commun Theor Phys*, 77(8):085801. https://doi.org/10.1088/1572-9494/adb5f4

Tah FA, Tabi CB, Kofane TC, 2021. Pattern formation in the Fitzhugh–Nagumo neuron with diffusion relaxation. *Chaos Sol Fract*, 147:110974. https://doi.org/10.1016/j.chaos.2021.110974

Tian QL, Shan XY, Bian JY, et al., 2025. Metal oxide-based resistive switching memristors for neuromorphic computing. *J Mater Chem C*, 13(24):12046-12065. https://doi.org/10.1039/D5TC01467K

Tomassoli L, Silva-Dias L, Dolnik M, et al., 2024. Neuromorphic engineering in wetware: discriminating acoustic frequencies through their effects on chemical waves. *J Phys Chem B*, 128(5):1241-1255. https://doi.org/10.1021/acs.jpcb.3c08429

Wang BC, Lv M, Zhang XF, et al., 2024. Dynamics in a light-sensitive neuron with two capacitive variables. *Phys Scr*, 99(5):055225. https://doi.org/10.1088/1402-4896/ad37b1

Wang BC, Ren GD, Ma J, et al., 2025. A memristive neuron with double capacitive variables coupled by Josephson junction. *Chaos Sol Fract*, 198:116630. https://doi.org/10.1016/j.chaos.2025.116630

Wang HL, Zhang DJ, Qian YH, 2025. Synchronization of bursting oscillations in coupled FitzHugh–Nagumo neurons. *Appl Math Model*, 147:116219. https://doi.org/10.1016/j.apm.2025.116219

Wang X, Mou J, Cao YH, et al., 2025. Modeling and analysis of cellular neural networks based on memcapacitor. *Int J Bifurc Chaos*, 35(4):2530010. https://doi.org/10.1142/S0218127425300101

Wang XQ, Yu D, Wu Y, et al., 2023. Effects of potassium channel blockage on inverse stochastic resonance in Hodgkin–Huxley neural systems. *J Zhejiang Univ Sci A*, 24(8):735-748. https://doi.org/10.1631/jzus.A2200625

Xie Y, Wang XQ, Li XN, et al., 2024. Energy consumption in the synchronization of neurons coupled by electrical or memristive synapse. *Chin J Phys*, 90:64-82. https://doi.org/10.1016/j.cjph.2024.05.033

Yamakou ME, Zhu JJ, Martens EA, 2024. Inverse stochastic resonance in adaptive small-world neural networks. *Chaos*, 34(11):113119. https://doi.org/10.1063/5.0225760

Yanagita T, Ichinomiya T, Oyama Y, 2005. Pair of excitable FitzHugh–Nagumo elements: synchronization, multistability, and chaos. *Phys Rev E*, 72(5):056218. https://doi.org/10.1103/PhysRevE.72.056218

Yang FF, Zhou P, Ma J, 2024a. An adaptive energy regulation in a memristive map linearized from a circuit with two memristive channels. *Commun Theor Phys*, 76(3): 035004. https://doi.org/10.1088/1572-9494/ad260e

Yang FF, Ma J, Wu FQ, 2024b. Review on memristor application in neural circuit and network. *Chaos Sol Fract*, 187:115361. https://doi.org/10.1016/j.chaos.2024.115361

Yang FF, Song XL, Yu ZH, 2024c. Dynamics of a functional neuron model with double membranes. *Chaos Sol Fract*, 188:115496. https://doi.org/10.1016/j.chaos.2024.115496

Yang FF, Ren LJ, Ma J, et al., 2024d. Two simple memristive maps with adaptive energy regulation and digital signal process verification. *J Zhejiang Univ Sci A*, 25(5): 382-394. https://doi.org/10.1631/jzus.A2300651

Yu ZH, Zhu KL, Wang Y, et al., 2025. Dynamics of a neuron with a hybrid memristive ion channel. *Chaos Sol Fract*, 194:116233. https://doi.org/10.1016/j.chaos.2025.116233

Zamani AP, Novikov N, Gutkin B, 2020. Concomitance of inverse stochastic resonance and stochastic resonance in a minimal bistable spiking neural circuit. *Commun Nonl Sci Numer Simul*, 82:105024. https://doi.org/10.1016/j.cnsns.2019.105024

Zheng CY, Peng L, Eshraghian JK, et al., 2022. Spiking neuron implementation using a novel floating memcapacitor emulator. *Int J Bifurc Chaos*, 32(15):2250224. https://doi.org/10.1142/S0218127422502248

Zidan MA, Strachan JP, Lu WD, 2018. The future of electronics based on memristive systems. *Nat Electron*, 1:22-29. https://doi.org/10.1038/s41928-017-0006-8